frontiers | Frontiers in Ecology and Evolution

TYPE Original Research
PUBLISHED 04 November 2022
DOI 10.3389/fevo.2022.1050429



OPEN ACCESS

EDITED BY
Xiaofeng Cao,
Tsinghua University, China

REVIEWED BY
Shailesh Agrawal,
Birbal Sahni Institute of Palaeosciences (BSIP), India
Mingkun Li,
South China Normal University, China

*CORRESPONDENCE
Chunmei Ma
chunmeima@nju.edu.cn

SPECIALTY SECTION
This article was submitted to Paleoecology, a section of the journal Frontiers in Ecology and Evolution

RECEIVED 21 September 2022
ACCEPTED 17 October 2022
PUBLISHED 04 November 2022

CITATION
Huang M, Deng Y, Peng H, Wen Z, Shang G, Guan H and Ma C (2022) Hydroclimatic changes since the Last Glacial Maximum recorded in mountain peat deposit on the southwestern margin of the Sichuan Basin, China. *Front. Ecol. Evol.* 10:1050429. doi: 10.3389/fevo.2022.1050429



# Hydroclimatic changes since the Last Glacial Maximum recorded in mountain peat deposit on the southwestern margin of the Sichuan Basin, China

Ming Huang[1,2], Yunkai Deng[1,3], Haijun Peng[4,5], Zhenming Wen[1], Guangchun Shang[1], Houchun Guan[6] and Chunmei Ma[1,7]*

[1]School of Geography and Ocean Science, Nanjing University, Nanjing, China, [2]Chengdu Institute of Cultural Relics and Archaeology, Chengdu, China, [3]Key Laboratory of Cenozoic Geology and Environment, Institute of Geology and Geophysics, Chinese Academy of Sciences, Beijing, China, [4]State Key Laboratory of Environmental Geochemistry, Institute of Geochemistry, Chinese Academy of Sciences, Guiyang, China, [5]CAS Center for Excellence in Quaternary Science and Global Change, Xi'an, China, [6]Geological Survey of Anhui Province, Hefei, China, [7]Jiangsu Collaborative Innovation Center for Climate Change, Nanjing, China

Knowledge of the hydroclimatic changes in Southwest China since the Last Glacial Maximum (LGM) is crucial for disentangling the long-term evolution of the Asia Monsoon and predicting the future fate of the mountain peat deposit in the Asia Monsoon region. In this study, we obtained a 530-cm-long peat core from the Ganchi wetland in Southwest China and analyzed its geochemical indices, including total nitrogen (TN), total organic carbon (TOC), stable carbon isotope composition of organics ($\delta^{13}$Corg), and the concentration of several major elements, to investigate the sedimentary and hydroclimate evolution since the LGM. We found that the peat strata in the Ganchi wetland have developed gradually from 13.7 cal kyr BP, which is likely ascribed to the warm climate during the Bølling-Allerød (B/A) period. TOC, $\delta^{13}$Corg, K/Ti, and Fe/Mn records showed notable paleoclimate shifts since the last deglaciation. The first warming period after the LGM was observed starting at 18.2 cal kyr BP, which is consistent with other records from Southwest China. The reconstruction results show that the western margin of the Sichuan Basin during the last deglaciation was most affected by the East Asia summer monsoon (EASM), and less affected by the Indian summer monsoon (ISM). The climate of the early Holocene (11.2–7.5 cal kyr BP) was

affected by both the ISM and EASM, resulting in more complex local climatic features. The Holocene Megathermal period observed from 7.5 to 3.5 cal kyr BP, is consistent with the timing detected in other records of Southwest China.

KEYWORDS

**Last Glacial Maximum, Southwest China, hydroclimate, Indian summer monsoon, peat record**

## Introduction

Southwest China is one of the most susceptible areas to climate changes owing to its diverse geomorphology that is adjacent to the Qinghai-Tibetan Plateau (QTP) and influenced by the East Asia summer monsoon (EASM) and the Indian summer monsoon (ISM) (Zhang, 1988; Zheng and Li, 1990; Zhang et al., 2015b; Liu, 2016). The climate of Southwest China, being superimposed by a series of abrupt warming/cooling events at a millennial to centennial timescale, has undergone long-term warming since the Last Glacial Maximum (LGM) (Alley and Clark, 1999; Shakun and Carlson, 2010). Many studies have focused on exploring the duration and mechanisms of warm and cold changes since LGM (Clark et al., 2009; Denton et al., 2010). However, the mechanism of abrupt climate changes in Southwest China since the LGM remains poorly explored due to the low number of geological archives. For instance, it is still debated whether Heinrich 1 (H1), Bøllinge-Allerød (B/A), and Younger Dryas (YD) events have been adequately detected in the paleoclimatic records in Southwest China (Shen and Xiao, 2018). Thus, more archives that cover the LGM from Southwest China are desired for a better understanding of the long-term hydroclimatic changes and driving mechanisms in this region.

Sichuan Basin in Southwest China, located on the southwestern margin of the QTP and adjacent to the Yunnan-Guizhou Plateau, has a population of over 100 million and was the cradle of many ancient Chinese civilizations such as the Sanxingdui culture and the Baodun culture (Huo, 2022). However, most of the paleoclimate reconstructions in Southwest China are concentrated in the Yunnan-Guizhou Plateau. While the majority of these researches were based on lake sediments (Cook et al., 2012; Wang et al., 2014; Xiao et al., 2014a; Wu et al., 2015; Zhang et al., 2015a; Zhang et al., 2017, 2018) and cave stalagmites (Dykoski et al., 2005), studies on peat core records are still minimum (Zhu et al., 2010; Gong et al., 2019; Liu et al., 2022). Besides, most of these researches only cover the last deglaciation or Holocene period, and studies on the LGM are relatively scarce (Devry, 1993; Hong et al., 2014; Peng et al., 2021). The relationship between monsoon evolution and paleoclimatic variability since the LGM in this area is still unclear both temporally and spatially.

Organic matter in peat is mainly derived from the continuous and stable stratigraphic accumulation of local plant residues. Since the vegetation combination varies in response to climate variability, it is thus expected that the development of peatland and its succession processes have recorded changes in the surrounding environment, regional climate, and dominant vegetation (Blackford, 2000; Chambers and Charman, 2004; Xu et al., 2006; Zhao et al., 2011, 2016; Chambers et al., 2012; Zhou et al., 2002). Alpine peat and lake sediment records in the southwest Sichuan Basin have shown several abrupt changes that may associate with the climate changes in the high northern latitudes (Hong et al., 2014; Peng et al., 2021). However, the locations of these records are a bit far away from the Sichuan Basin and are often affected by the local climate of Hengduan Mountain. To investigate the complexity of the climate in the Sichuan Basin since the LGM, more archives that are adjacent to or within the Sichuan basin are needed. Here we present a study of the stable carbon isotope composition of organics ($\delta^{13}$Corg), total nitrogen (TN), total organic carbon (TOC), and element geochemistry of a 26,200 years old peat archive from Dawa Mountain, which is located at the west margin of Sichuan Basin. The objectives of this study are (1) to investigate the environmental evolution of peatland near the Sichuan Basin since the LGM, (2) to reconstruct the LGM hydroclimate of the Sichuan Basin, and (3) to explore the links between abrupt environmental/climate changes and historical civilizations in Southwest China.

## Materials and methods

### Coring and sampling

Dawa Mountain, located in the southern part of Sichuan Province, China, is situated in the transition zone between the southwest margin of the Sichuan Basin and the Yunnan-Guizhou Plateau. The landform of this region is dominated by scattered karst landforms, such as karst basins and corrosion lakes. The Dawa Mountain region has gentle topographical relief and is not significantly affected by runoff erosion (Luo, 2003; Wang and Chen, 2014). The Ganchi wetland (29°23′ 69The Gan°1′ 54The Ganchi wet1,805 m) was formed due to this

topography and its high precipitation. The peat strata in Ganchi of Dawa Mountain was formed by the paludification of karst wetland, with no riverine input from its surrounding (**Figure 1**).

A 530-cm-long peat core (GC) was collected from the middle of Ganchi wetland using a Russian peat corer. The 50-cm long peat cores were packaged into PVC tubes and transported to the laboratory. These peat cores were sliced into 1-cm intervals, resulting in a total of 530 samples. The strata were divided into five layers based on the sedimentary characteristics: (1) 0–10 cm: dark- brown peat topsoil with abundant grass roots; (2) 10–230 cm: dark-brown peat containing a large number of undecomposed plant roots; (3) 230–380 cm: dark-gray peat with a small number of plant roots; (4) 380–505 cm: gray-black peat mixed with clay; (5) 505–530 cm: Light gray clay mixed with sand and gravel (the bottom of this layer was close to the bedrock).

## Methods

### Dating

Both plant fragments and pollen residues were extracted from the peat samples for radiocarbon dating. A total of 14 samples were selected from different depths of the GC core for AMS$^{14}$C dating based on the stratum lithology. Eleven and three samples were tested at the Xi'an Accelerator Mass Spectrometry Center, Institute of Earth Environment, Chinese Academy of Sciences, and Beta analytic Inc., respectively. The age data was then calibrated to calendar ages using Calib7.0.4 (Reimer et al., 2013). The winbacon2.2 R package (Blaauw and Christen, 2011) based on the Bayes formula was used to establish an accurate and complete age-depth model for the GC core and to calculate the deposition rate (**Figure 2**).

### Elemental geochemistry

After being transported to the lab, the GC core was first tested using the non-destructive X-ray fluorescence (XRF) core scanning technic, which is a widely used in stratigraphic comparison and paleoclimate research across different depositional environments (Haug et al., 2001; Kido et al., 2006; Cuven et al., 2010; Cheng et al., 2011; Hennekam and de Lange, 2012; Liang et al., 2012; Peros et al., 2017). Major element compositions in the GC core were measured by an Avaa-tech system in the Key Laboratory of Surficial Geochemistry, Ministry of Education, Nanjing University. During the analysis, scanning voltages of 10 KV and 30 KV were selected at a resolution of 1 cm, and the samples were scanned for 10 s to obtain the counts of Ti, K, Si, Al, Fe, Mn, Sr, Zr, Ca, S, and Cl. The elemental concentration results were considered semi-quantitative due to the influence of core water content, grain size, cracks, and surface flatness on the X-ray (Weltje and Tjallingii, 2008).

### Total organic carbon, total nitrogen, and $\delta^{13}C_{org}$ analysis

A total of 265 samples were selected at 2-cm intervals for the TOC, TN, and $\delta^{13}C_{org}$ analysis. The pretreatment and measuring were conducted in the Key Laboratory of Surficial Geochemistry, Ministry of Education, Nanjing University. The selected samples were firstly oven-dried, and then grounded and sieved using an 80-mesh sieve. The samples were then treated with 10% HCl for 24 h to remove carbonates. Subsequently, the samples were washed with distilled water to achieve neutrality and dried at low temperature. For TOC and TN measurements, 50 mg of the pre-treated samples were weighed and then tightly wrapped in tin foil and then loaded into the VarioMacro-CHNS elemental analyzer. Phenylalanine was used as the standard sample, and a national standard (GBW04408) was analyzed after 5 samples for quality control of the instrument. The instrument had an analytical accuracy of 0.5%. The ratio of TOC to TN (C/N) was calculated based on the contents of TOC and TN. $\delta^{13}C_{org}$ was determined using a Picarro laser spectrum carbon isotope analyzer (G2131-i). The carbon isotope results are expressed as the per mil (‰) deviation from Vienna Pee Dee Belemnite (VPDB), with a precision of less than 0.3%.

## Results

### Chronology and sedimentation rate

The AMS$^{14}$C data of the GC core are shown in **Table 1**, and the age-depth model and sedimentation rate are shown in **Figure 2**. The sedimentation rate of the GC core varied greatly at different depths. The average sedimentation rate of the whole core was 27 cm/kyr. The maximum deposition rate (average of 48 cm/kyr) occurred at 107–226 cm depth, and the minimum deposition rate (average of 8.9 cm/kyr) occurred at 282–365 cm depth. Overall, the sedimentation rate varied significantly during the Holocene, but showed little variability from the LGM to the Holocene.

### Scanning X-ray fluorescence results

As shown in **Figure 3**, the variation trends in Al, Ti, and Fe concentrations were similar, while the trends of Si and Mn showed low variability. The changes in these elements and the Al/Si ratio can be divided into three stages. The first stage is the LGM (26.2–18.2 cal kyr BP, 530–372 cm), which can be divided into two sub-stages: Stage I-1 (26.2–25.2 cal kyr BP, 530–505 cm) and Stage I-2 (25.2–18.2 cal kyr BP, 505–372 cm). In Stage I-1, all indexes fluctuated sharply, and in stage I-2, Al, Ti, Mn, and Cl are relatively stable, while other elements and ratios fluctuated slightly. In stage II (18.2–11.2 cal kyr BP, 372–310 cm), Si and Mn remained stable, the strength

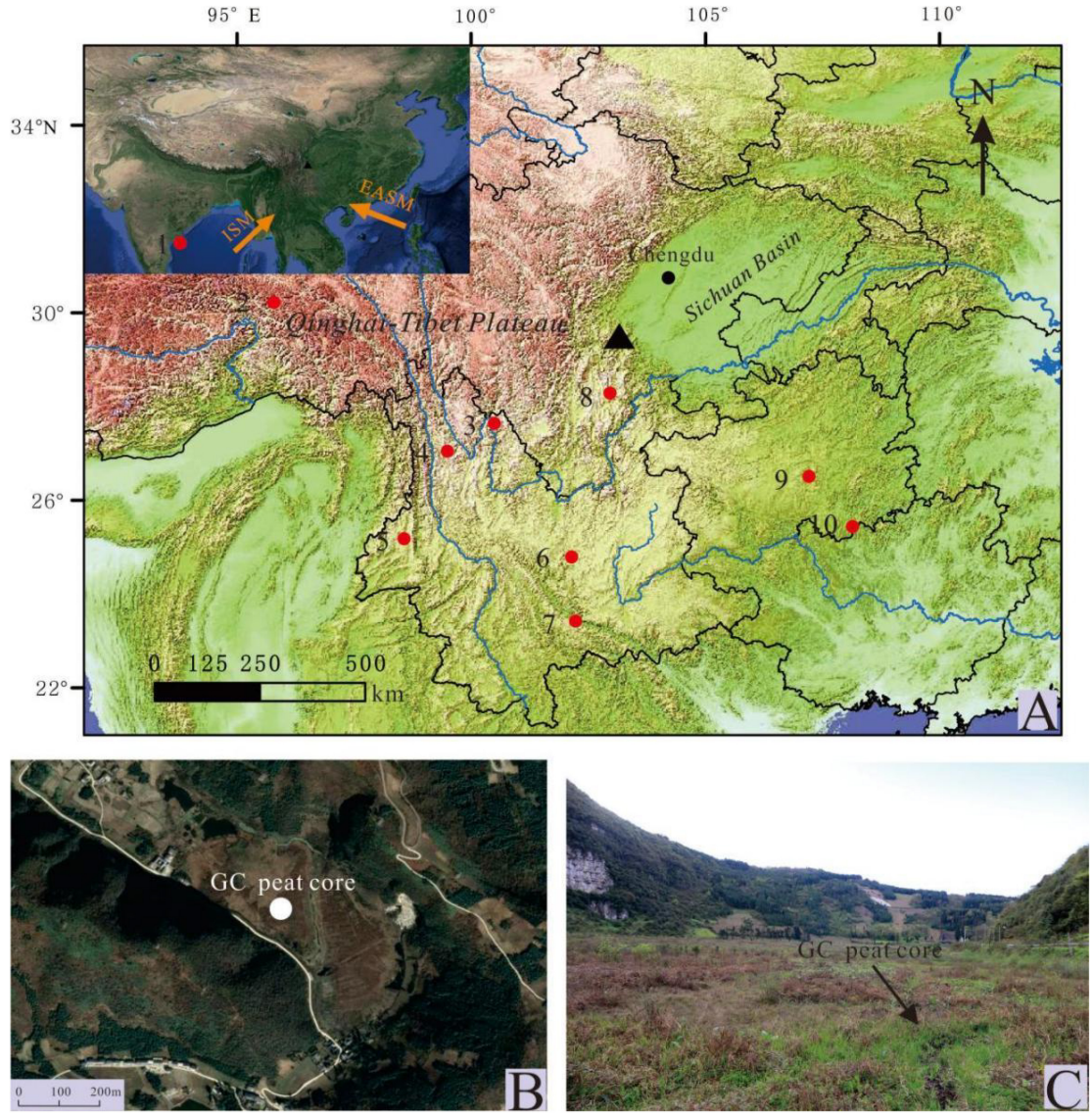


FIGURE 1
Locations of the research area and the related research sites. **(A)** Map of the research area indicating the location of the peat site (black triangle) at the intersection between the Sichuan Basin, Yunnan-Guizhou Plateau, and QTP. The red circles indicate the location of related research sites cited in this study: (1) Core SK218 in the Indian Ocean (Govil and Divakar Naidu, 2011); (2) core NC08/01 in Nam Co Lake on the QTP (Zhu et al., 2015); (3) core LG08 in Lugu Lake, Yunnan Province (Zhang et al., 2018); (4) core TCYL1 in Tiancai Lake, Yunnan Province (Xiao et al., 2014b); (5) core TCK1 in Qinghai Lake, Tengchong County, Yunnan Province (Xiao et al., 2015); (6) core XY08A in Xingyun Lake, Yunnan Province (Wu et al., 2015); (7) core from Yilong Lake, Yunnan Province (Li et al., 2018); (8) Baoan peat core in Sichuan Province (Hong et al., 2018); (9) peat borehole NT03 in Caohai, Guizhou Province (Gong et al., 2019); and (10) stalagmites in Dongge Cave, Guizhou Province (Dykoski et al., 2005). **(B)** Aerial photo of the Ganchi wetland with the location of the GC core shown as a solid white circle; and **(C)** a physical picture shows the geomorphic environment around the sampling site.

of other elements was significantly enhanced, and the Si/Al value gradually increased. In stage III (since 11.2 cal kyr BP, 310–0 cm), the element strength remained relatively stable, but showed great fluctuations at time nodes such as 9.0 kyr BP and 6.0 kyr BP. The Si/Al ratio reaches the maximum value of the profile at this stage.

The correlations between the analyzed elements are shown in Table 2. The correlations between Zr, Sr, Si, Fe, K, Ti, Mn, and Al were generally high, and the correlation coefficients of Zr, Sr, Si, Fe, K, and Ti are above 0.6. While S, Cl, and Ca showed low correlation with other elements, Cl was the only element that negatively correlated with the other elements. The factor analysis results identified three principal components controlling the deposition of chemical elements, with a cumulative contribution rate of 83.5% to the total variance (Figure 4). Factor 1 contributed 57.0% to the total

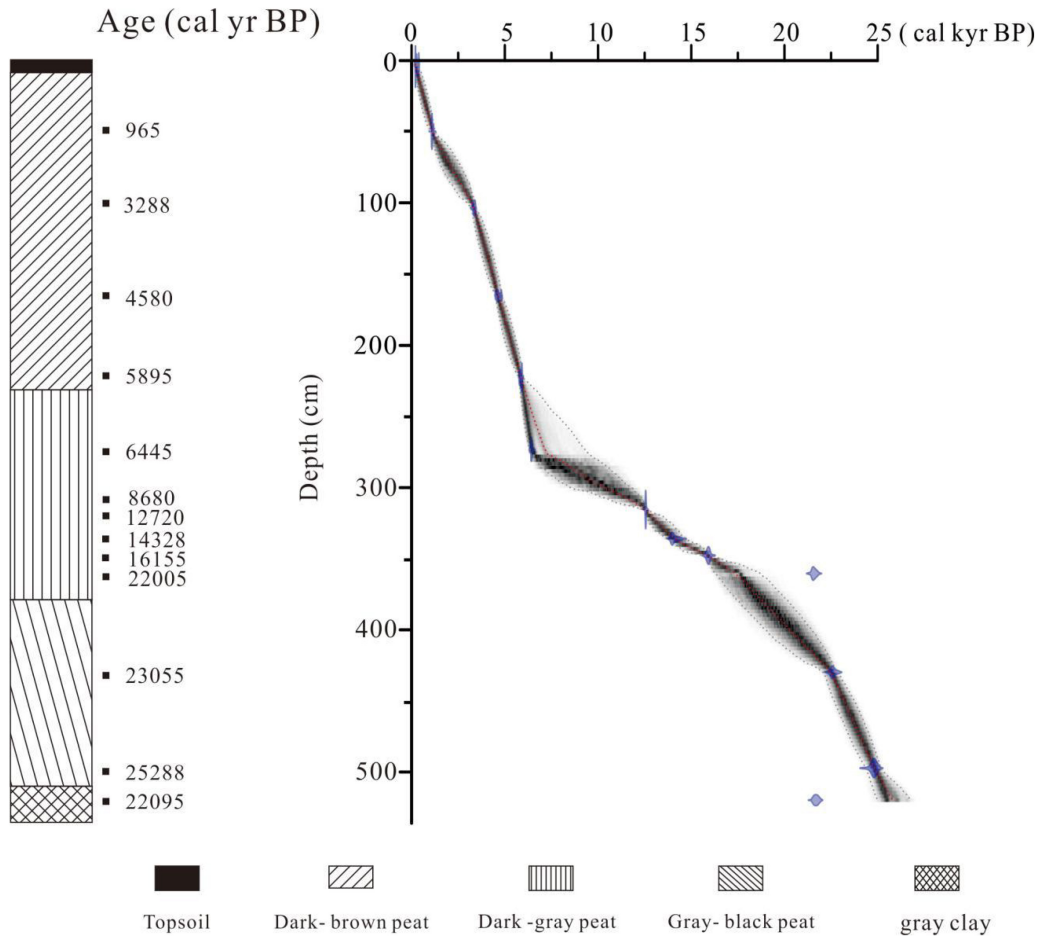


FIGURE 2
Stratigraphy and age-depth model of the GC core.

TABLE 1 AMS$^{14}$C dating results of the GC core.

| Lab. code | Depth(cm) | Materials | $^{14}$C data (a BP) | Error (±a) | Calibrated age (cal a BP, 2σ) | Mid-point (cal a BP) |
|---|---|---|---|---|---|---|
| XA19958 | 1 | Plant fragments | 65 | 20 | – | – |
| XA19949 | 49 | Plant fragments | 1,060 | 25 | 930–1,000 | 965 |
| XA19959 | 104 | Plant fragments | 3,070 | 30 | 3,210–3,365 | 3,288 |
| XA19960 | 167 | Plant fragments | 4,080 | 35 | 4,510–4,650 | 4,580 |
| XA19961 | 226 | Plant fragments | 5,125 | 30 | 5,860–5,930 | 5,895 |
| XA19950 | 278 | Plant fragments | 5,655 | 30 | 6,390–6,500 | 6,445 |
| Beta-565627 | 314 | Pollen residue | 7,870 | 30 | 8,589–8,770 | 8,680 |
| XA19951 | 321 | Plant fragments | 10,820 | 40 | 12,680–12,760 | 12,720 |
| Beta-565624 | 342 | Pollen residue | 12,290 | 60 | 14,029–14,626 | 14,328 |
| Beta-565625 | 354 | Pollen residue | 13,430 | 40 | 15,983–16,324 | 16,155 |
| XA19952 | 367 | Plant fragments | 18,130 | 65 | 21,780–22,230 | 22,005 |
| XA19962 | 438 | Plant fragments | 19,105 | 70 | 22,770–23,340 | 23,055 |
| XA19947 | 507 | Plant fragments | 20,940 | 100 | 25,000–25,575 | 25,288 |
| XA19948 | 530 | Plant fragments | 18,230 | 75 | 21,860–22,330 | 22,095 |

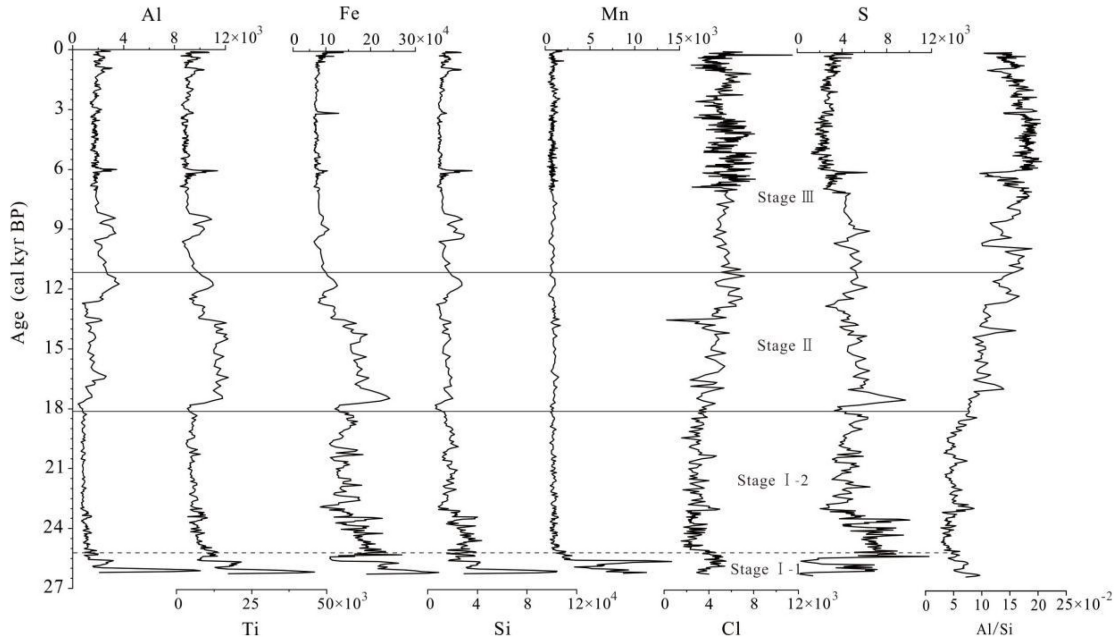


FIGURE 3
Scanning intensity and chromaticity curves of elements from the GC core.

TABLE 2 Correlation coefficients between elements in the GC core.

| | Sr | Zr | Al | Si | S | Cl | K | Ca | Ti | Mn | Fe |
|---|---|---|---|---|---|---|---|---|---|---|---|
| Sr | 1 | | | | | | | | | | |
| Zr | 0.900** | 1 | | | | | | | | | |
| Al | 0.171** | 0.374** | 1 | | | | | | | | |
| Si | 0.612** | 0.680** | 0.524** | 1 | | | | | | | |
| S | 0.476** | 0.288** | −0.245** | 0.399** | 1 | | | | | | |
| Cl | −0.428** | −0.364** | 0.248** | −0.372** | −0.364** | 1 | | | | | |
| K | 0.702** | 0.821** | 0.611** | 0.864** | 0.143** | −0.277** | 1 | | | | |
| Ca | 0.512** | 0.518** | 0.133** | 0.374** | 0.047 | −0.310** | 0.526** | 1 | | | |
| Ti | 0.836** | 0.866** | 0.533** | 0.804** | 0.350** | −0.262** | 0.902** | 0.396** | 1 | | |
| Mn | 0.497** | 0.654** | 0.469** | 0.636** | −0.014 | −0.134** | 0.804** | 0.494** | 0.679** | 1 | |
| Fe | 0.775** | 0.699** | 0.073 | 0.765** | 0.682** | −0.474** | 0.718** | 0.316** | 0.805** | 0.541** | 1 |

**Significantly correlated at 0.01 level (bilaterally).

variance and was therefore the main influencing factor in the GC core. Factor 2 and Factor 3 contributed 17.4 and 9.1% to the total variance, respectively. S and Fe had a high common factor load in Factor 2, while Ca and Cl had a high common factor load in Factor 3.

## Total organic carbon, total nitrogen, and $\delta^{13}$Corg

The GC record can be divided into the same three stages as **Figure 3** based on the various characteristics of TOC, TN, C/N, and $\delta^{13}$Corg (**Figure 5**). In Stage I-1 (26.2–25.2 cal kyr BP, 530–505 cm), the indicators fluctuated sharply, with average TN and TOC values being 0.3 and 4.2%, respectively. The average values of C/N and $\delta^{13}$Corg were 22.7 and –18.6‰, respectively, which were the maximum values in the core. At Stage I-2 (25.2–18.2 cal kyr BP, 505–372 cm), TN was relatively stable, with an average value of 1.1%. TOC and C/N values showed an increasing trend but remained relatively low, with average values of 15.1% and 13.8, respectively. In addition, $\delta^{13}$Corg showed an increasing trend throughout the entire stage, with an average value of –23.4‰.

Stage II represents the last deglaciation (18.2–11.2 cal kyr BP, 372–310 cm), during which the TN, TOC, and C/N values showed an overall increasing trend with average values of 1.3%,

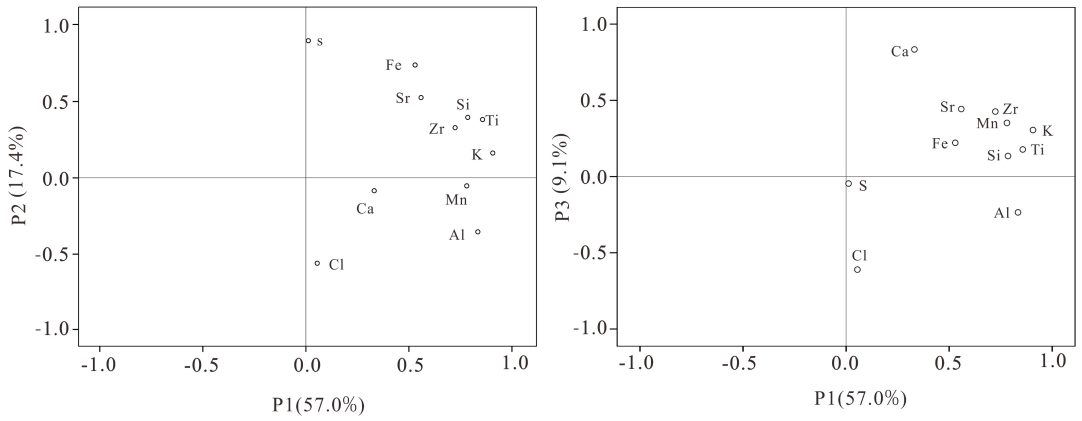


FIGURE 4
Factor analysis component loads of elements in the GC core.

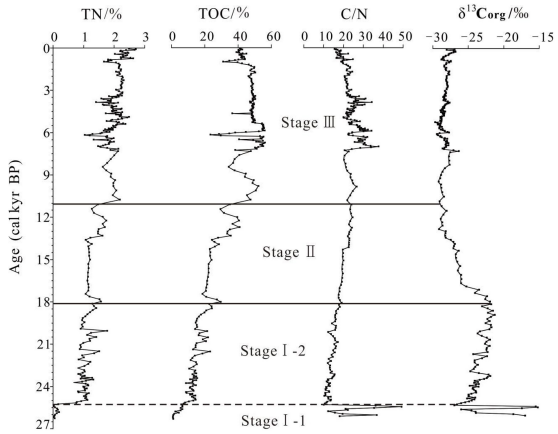


FIGURE 5
$\delta^{13}$Corg, TN, TOC, and C/N curves in the GC core.

28.7%, and 21.1, respectively. The $\delta^{13}$Corg values were generally more negative with an average value of –27‰.

Stage III was the Holocene (since 11.2 cal kyr BP, 310–0 cm), during which the average values of TN, TOC, and C/N were 2%, 47%, and 23.7, respectively; the $\delta^{13}$Corg values were more negative, with an average value of –28.4‰.

# Discussion

## Sediment and organic matter sources

Lake and wetland sediments have two dominant sources: (1) Exogenous components via erosion in the basin, and (2) endogenous precipitation produced by chemical and biological processes in the lake (Hakanson and Jansson, 2002; Shen, 2013). The correlation between elements is controlled by their geochemical behavior in the supergene environment. The source of substances can therefore be distinguished by the correlation between different elements, where a high correlation indicates similar occurrence conditions and sources of elements (Loring and Asmund, 1996; Ma et al., 2014). Factor analysis can also determine the source and contribution of geochemical elements in the sediments (Lawrence and Upchurch, 1982; Yang and Li, 1999; Zhang et al., 2015c). The loading values of, Al, Mn, Si, K, Ti, and Zr in Factor 1 in the GC core were relatively high, which is consistent with the results of the correlation analysis (**Figure 4**). These elements are rock-forming elements that are mostly transported and deposited in lakes by runoff in the form of terrigenous debris (Cheng et al., 2011; Wu et al., 2011). Therefore, exogenous detritus was likely the main source of the GC core sediments.

TOC generally indicates the level of organic matter in wetland sediments. Moreover, TOC can indicate the productivity of wetlands and their preservation ability in sediments (Meyers and Lallier-Vergès, 1999). TOC sources can be divided into exogenous terrestrial plants and endogenous aquatic plants, which can be roughly determined by the C/N ratio. C/N ratio that is smaller than 10 suggests that organic matter was mainly derived from algae and planktonic organisms and submerged and emergent plants in lakes (Meyers, 1997; Meyers and Lallier-Vergès, 1999); A C/N ratio greater than 20 suggests that the main organic matter source was terrestrial higher plants (Meyers, 1994; Talbot and Laerdal, 2000; Lamb et al., 2006; Morrill et al., 2006; Díaz et al., 2017). Our record higher than 20 for most samples shows that terrestrial higher plants are the dominant source of TOC in the Ganchi wetland.

Different plants exhibit different $\delta^{13}$Corg values. For example, C3 plants exhibit a $\delta^{13}$Corg value between –32 and –20‰, with the highest frequency being –27‰; meanwhile, C4 plants exhibit a $\delta^{13}$Corg value between –15 and –9‰, with the highest frequency being –13‰ (O'Leary, 1981, 1988;

Zhou et al., 2016). The $\delta^{13}$Corg values of submerged plants range from –20 to –12‰, with an average of –15%, which is close to the average $\delta^{13}$Corg value of C4 plants (–14‰). Finally, the $\delta^{13}$Corg values of emergent plants are between –30 and –24‰ (Lei et al., 2014). The $\delta^{13}$Corg value in sediments is therefore sensitive to the changes in organic matter sources and vegetation.

The $\delta^{13}$Corg value during the LGM Stage 1–1 (26.2–25.2 cal kyr BP) was relatively higher values (average value of –18.6‰, **Figure 6**), inferring the dominance of submerged plants. The $\delta^{13}$Corg values of the other stages were relatively more negative (average value of –28.1‰), which is consistent with the sediment isotope values in Caohai (Gong et al., 2019) and Lugu Lake (Zhang et al., 2018). The vegetation features in these areas are dominated by C3 plants, which suggests that the vegetation in Ganchi expands to C3 plants after 25.2 cal kyr BP. The average C/N of the GC core was > 10, especially after ∼13.7 cal kyr BP (∼23.6), which suggests that terrestrial plants were the dominant source of sedimentary organic matter. This also indicates the transition from a lake to a swamp environment in Ganchi after 13.7 cal kyr BP.

The above findings are in good agreement with the results of the major element concentrations. After ∼13.7 cal kyr BP, the intensity of Ti, Zr, and other elements related to exogenous output in Factor 1 gradually decreased (**Figure 3**). Due to the difference in the redox conditions between Fe and Mn, the Fe/Mn ratio can be used to evaluate the redox conditions of sediments. A higher Fe/Mn value indicates an unfavorable redox environment for oxidation, reflecting a deeper water environment. In contrast, a lower value indicates oxidation environments of shallower water levels (Wersin et al., 1991; Meng et al., 2018). We observed a high Fe/Mn ratio before 13.7 cal kyr BP (**Figure 6**), which then decreased sharply, reflecting a significant decline in the water level at approximately 13.7 cal kyr BP. Ti is a representative element of exogenous clastic sediments. The strength of the Ti element also began to decrease significantly during this stage (**Figure 3**), which may be ascribed to the decreased contribution of exogenous clastic sediments after the drying of the lake basin.

As Ganchi has a relatively closed topography without any notable river input, the presence of exogenous clastic sediments in the GC core was likely caused by the fluctuation of the lake water level, which transported exogenous clastic sediments to the coring site. After gradual paludification, the exogenous clastic sediments were likely transported to Ganchi by temporary sheet flow or surface runoff.

## Response of total organic carbon and $\delta^{13}$Corg to paleoclimatic changes

In the monsoon climate region, climate changes significantly influence the formation and development of peat. Previous studies have shown that the monsoon and sunlight are important factors affecting the expansion of peatlands in the Hengduan Mountains (Liu et al., 2020), and the humid monsoon climate is also conducive to peatland expansion (Xing et al., 2015). TOC content in peatland sediments is closely related to the accumulation of organic matter, which can reflect the development of peatlands. The TOC records from the Dajiuhu peatland at a latitude similar to Ganchi indicated the close relationship between TOC and EASM strength, with higher TOC correlating with stronger EASM (Zhang, 2017). The TOC records of the Zoige and Hongyuan peatlands in the southeastern margin of the Tibetan Plateau also reflected the Holocene monsoonal changes (Zhou et al., 2002; Wang et al., 2010). The Ganchi sedimentary environment transitioned from a lake to a wetland at ∼13.7 cal kyr BP, resulting in the gradual development of peat, which is consistent with the initial peak timing (14.5–13.0 cal kyr BP) of peat development in the Hengduan Mountain area due to the Bølling-Allerød warm climate (Liu et al., 2022). The variation trend of TOC in the GC core during the last deglaciation is consistent with the variation trend of monsoon intensity, as reflected by sunlight and stalagmite oxygen isotope records from Dongge and Hulu cave (Wang et al., 2001; **Figure 7C**). Therefore, the TOC variation in this study can be used as an indicator of the strength of the monsoon and the resulting paleoclimatic changes.

After 13.7 cal kyr BP, the TOC changes in the GC core were negatively correlated with Ti/Ca, Fe/Mn ratios and terrigenous clastic sediments, but positively correlated with a sedimentation rate (**Figure 6**). During the warm periods of 13.7–12.0 cal kyr BP and 7.5–3.5 cal kyr BP, the TOC and vegetation coverage increased, and the peat accumulation and deposition rates were more rapid (Liu et al., 2020). As the soil and water were effectively conserved, the amount of exogenous clastic sediments entering the dry pool via water inflow decreased. During the cold and dry periods of 12.0–11.2 cal kyr BP, 9.0 cal kyr BP, and 6.0 cal kyr BP, the vegetation coverage, TOC, peat accumulation rate, and deposition rate all decreased. During these cold and dry stages, the increase in detrital sediments in Ganchi may be related to the loss of soil and water and the increase of atmospheric dust deposition (Peng et al., 2021).

The $\delta^{13}$Corg values in wetland sediment core reflect both vegetation evolution and paleoclimatic changes. Moreover, the organic carbon isotope composition of plants reflects the type of photosynthesis, atmospheric $CO_2$ concentrations (Francey and Farquhar, 1982; Meyers and Ishiwatari, 1993), and climatic conditions (Hong et al., 2010; Xue et al., 2014). Therefore, the environmental signal reflected by the $\delta^{13}$Corg value is complex. In this study, the $\delta^{13}$Corg value was generally more negative during the last deglaciation, which is consistent with the variations in TOC and oxygen isotopes derived from Dongge cave and Hulu cave stalagmites, and with the $\delta^{13}$Corg trend from Baoan peatland, which reflects the variation in the Asian monsoon (**Figure 7**). Therefore, the $\delta^{13}$Corg trend and TOC

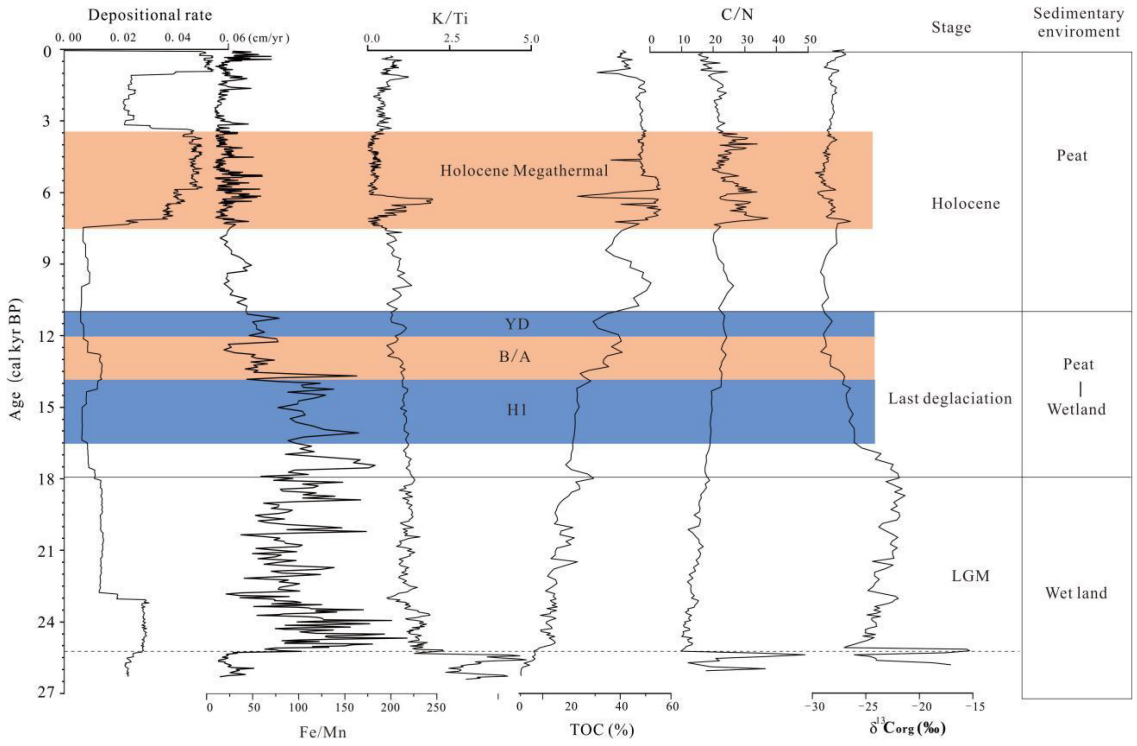


FIGURE 6
Comparison of paleoenvironmental indicators since the LGM in the GC core.

record in the GC core likely reflect monsoon intensity and the subsequent paleoclimate changes. The paleoenvironmental indicators in this study are consistent with the paleoclimate changes recorded by the GC core high-resolution pollen (Deng et al., 2022; **Figure 7A**).

## Depositional environmental and vegetation evolution since the Last Glacial Maximum in Ganchi

According to the changes in the paleoenvironmental proxies, the evolution of the depositional environment since the LGM (recorded in the GC core) in Ganchi can be divided into three stages (**Figure 6**): (1) the LGM (26.2–18.2 cal kyr BP), (2) last deglaciation (18.2–11.2 cal kyr BP), and (3) Holocene (since 11.2 cal kyr BP).

### Last Glacial Maximum (26.2–18.2 cal kyr BP)

**Figure 6** shows that the LGM stage can be divided into two sub-stages. During 26.2–25.2 cal kyr BP, the mean values of TOC, C/N, and $\delta^{13}$Corg were 4.2%, 22.7, and −18.6‰. Organic matter accumulation in the study area was less, mainly in terrestrial higher plants and submerged plants. During 25.2–18.2 cal kyr BP, the TOC value increased, the $\delta^{13}$Corg value reached −23.4‰, and the C/N value was between 10 and 20, which reflected the change of vegetation type in the study area., The contribution of C3 plants gradually increased and become dominant from this stage, but there were also some aquatic plants. The high Fe/Mn ratios indicate a wetland environment. The concentration of Ti, Zr, and other elements indicate the small fluctuation of exogenous clastic sediments, which infers a relatively stable sedimentary environment, with a low and less variable deposition rate.

### Last deglaciation (18.2–11.2 cal kyr BP)

In this stage, $\delta^{13}$Corg values showed a more negative trend (mean −27.0u), and TOC and C/N values exhibited increased fluctuations. Particularly from 13.7 cal kyr BP, the average C/N value was greater than 20, TOC increased significantly, and the intensities of Ti and Zr decreased significantly (**Figures 3**, **6**). This indicates that since 13.7 cal kyr BP, the exogenous clastic sediments in the study area decreased significantly; Terrestrial higher vegetation represented by C3 plants further increased, and various algae, phytoplankton, submerged macrophytes, and emergent macrophytes gradually decreased. The Fe/Mn ratio gradually decreased from 13.7 cal kyr BP, indicating a decreasing water level in Ganchi and the transition of the sedimentary environment from wetland to peatland. This is consistent with previous research results on the timing of peat development

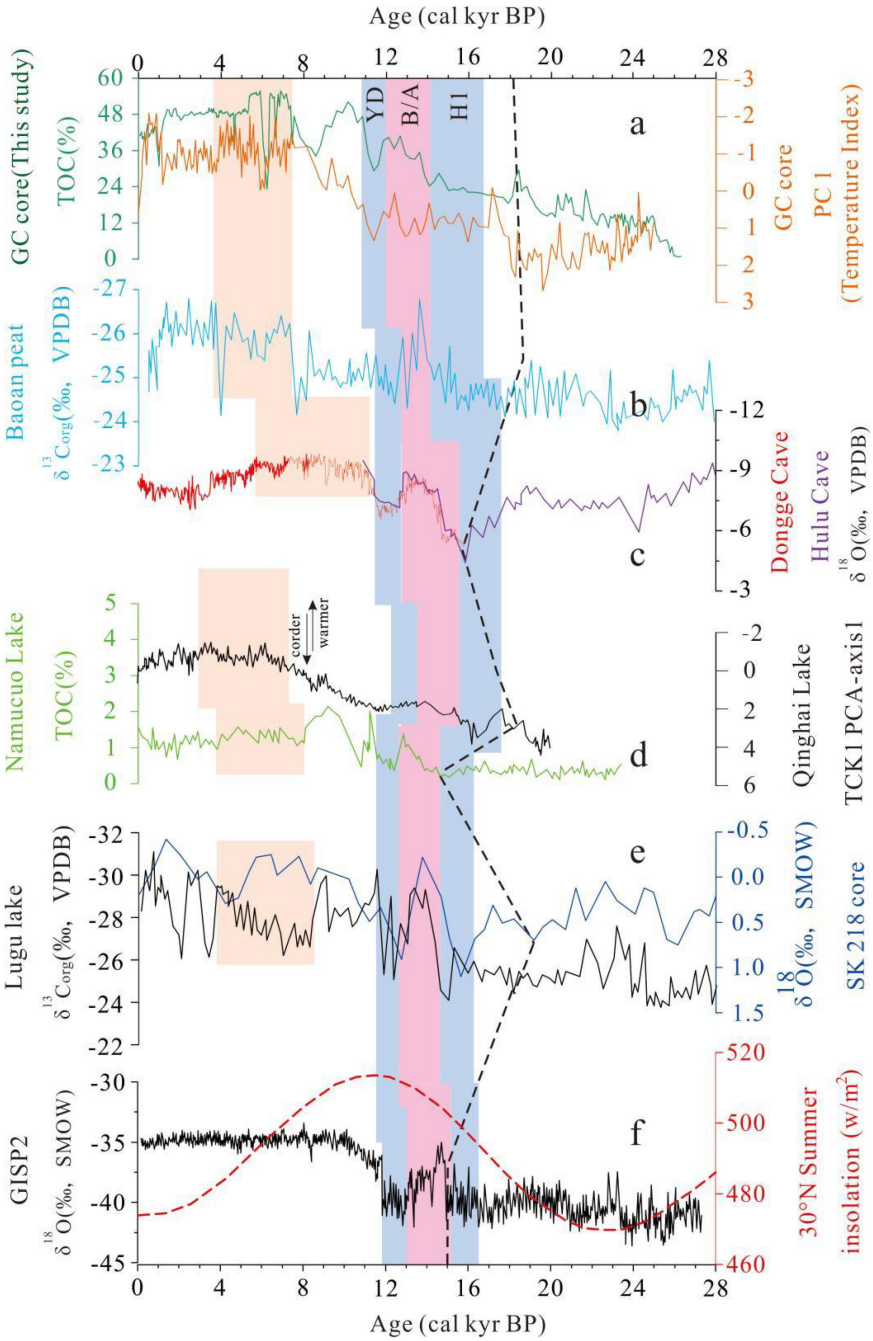


FIGURE 7
Comparison of the paleoenvironmental records in the GC core with that of other areas since the LGM. **(a)** Principal component1 (PC1) scores of the pollen in the GC core (orange curve, Deng et al., 2022), this curve can be used as temperature index, the higher the temperature, the smaller the value. TOC percentage content (green curve) of the GC core (this study); **(b)** $\delta^{13}$Corg records of the Baoan peat (Blue curve, Hong et al., 2018), **(c)** $\delta^{18}$O stalagmite record from Dongge Cave (red curve, Dykoski et al., 2005) and Hulu Cave (purple curve, Wang et al., 2001); **(d)** TOC percentage in sediment core NC08/01 from NamCo Lake, QTP (black curve, Zhu et al., 2015) and the PC1 scores of pollen in core TCK1 from Qinghai Lake, Tengchong (green curve, Xiao et al., 2015); **(e)** sea surface $\delta^{18}$O record from core SK218 in the Indian Ocean (blue curve, Govil and Divakar Naidu, 2011) and $\delta^{13}$Corg record in sediment core LG08 from Lugu Lake, Yunnan Province (black curve, Zhang et al., 2018); **(f)** 30° N summer insolation curve (red dotted line, Berger and Loutr, 1991) and $\delta^{18}$O record from the GISP2 ice core in Greenland (black curve, Stuiver and Grootes, 2000). The black dotted line indicates the first warming period after the LGM at different locations; the blue band indicates the H1 and YD cold events; and the pink band indicates the B/A warm period. The orange band indicates the Holocene Megathermal.

in the southern Hengduan Mountains, which mostly occurred before the Holocene (Liu et al., 2020).

### Holocene (since 11.2 cal kyr BP)

During the Holocene, the intensities of Si, Fe, K, and Ti were relatively low, indicating the lower transport of exogenous clastic sediments to the study area. TOC and C/N increased to maximum levels, and the $\delta^{13}$Corg (mean −28.4 ‰) was more negative, which suggests that terrestrial C3 plants were the dominant organic matter sources and that the Ganchi wetland had completely evolved into peatland.

## Paleoclimate evolution and driving mechanisms since the Last Glacial Maximum in the southern margin of the Sichuan Basin

### First warming period after the Last Glacial Maximum

Studies (Wang et al., 2014; Xiao et al., 2014a; Jin et al., 2015; Zhu et al., 2015; Li et al., 2018) have shown that the LGM climate in Southwest China was generally cold and dry, and the first period of warming after the LGM occurred between 19 and 17 kyr BP (Cook et al., 2012; Wu et al., 2015; Zhang et al., 2018). Similar paleoclimatic changes were recorded in the GC core. During the LGM, due to the cold and dry climate, the organic matter accumulation is less, the TOC was relatively low, and $\delta^{13}$Corg was relatively higher values. Since 18.2 cal kyr BP, the TOC increased significantly, and $\delta^{13}$Corg showed an obvious more negative trend, indicating a warming climate. Therefore, the timing of the first warming period after the LGM in Ganchi (the southern margin of the Sichuan Basin) was 18.2 cal kyr BP, which is consistent with the timing of the first warming period in Southwest China. However, the timing of the first warming in Southwest China notably differed from that recorded in the Northern Hemisphere high latitudes (Johnsen et al., 1992) and the EASM region (Wang et al., 2001), but was similar to that recorded in the Indian Ocean region (Govil and Divakar Naidu, 2011; **Figure 7E**). This suggests that the first warming in Southwest China was not controlled by the changes in the high-latitude ice sheets of the Northern Hemisphere but was likely related to the strengthening of the ISM caused by increasing solar radiation in 30°N since 21 kyr BP (**Figure 7F**), which further affected Southwest China (Shen and Xiao, 2018).

### Climate changes during the last deglaciation

The climate was generally warm in the study area during the last deglaciation (18.2–10.9 cal kyr BP), which was superimposed by several abrupt climate change events.

The most notable climate fluctuation occurred during 13.7–12.0 cal kyr BP and 12.0–11.2 cal kyr BP (**Figure 6**). The study area belongs to the carbonatite area. The K, Ca and other soluble elements in the carbonatite are easily leached and migrated, resulting in a relative loss of content, while the Ti element is relatively stable. Therefore, the K/Ti ratio can reflect the chemical weathering intensity of the study area, thus indicating climate change (Qu and Huang, 2019). During 13.7–12.0 cal kyr BP, the TOC increased significantly and the K/Ti ratio decreased, reflecting the warm climate and strong chemical weathering during this period, which likely indicates the Bølling-Allerød warm period in this region.

During the period of 16.5–13.7 cal kyr BP and 12–11.2 cal kyr BP, TOC and $\delta^{13}$Corg were decreased and biased, especially during the period of 12–11.2 cal kyr BP. The K/Ti ratio also increased significantly during 12–11.2 cal kyr BP. The changes in the above indicators reflect that there were relatively obvious climate cooling events in these two periods, which may correspond to H1 and YD events, respectively. Al/Si ratio can be used as an indicator of sediment particle size. In general, with higher Al/Si ratio indicating finer grain size (Bloemsma et al., 2012; Babek et al., 2015). In the above two periods, the Al/Si ratio showed obvious low values, which may mean that the cold and dry climate in these two periods, due to the low vegetation cover, flowing water erosion brought more coarse-grained sediments. These millennial-scale fluctuations are consistent with the $\delta^{18}$O records of the GISP2 ice core in Greenland (Stuiver and Grootes, 2000; **Figure 7F**), the SK218/1 core in the Bay of Bengal (Govil and Divakar Naidu, 2011; **Figure 7E**), and the Hulu cave stalagmite in eastern China (Wang et al., 2001; **Figure 7C**). The significant weakening of the ISM during the H1 and YD periods was also recorded in other lake sediments (Wang et al., 2014; Xiao et al., 2014b; Zhang et al., 2015a) and stalagmites (Dykoski et al., 2005) in Southwest China.

The climate change recorded in the GC core is similar to that observed in the records of Southwest China, except for the precise start and end time of the climate intervals and the degree of change. These differences may be related to the sensitivity of the different regions to climate change as well as the possible uncertainties in chronology (Shen and Xiao, 2018). In addition, due to the topography of the QTP, the climate of different regions in the southwest may be more complex and diverse. For example, the peat records of Caohai, south of the QTP, indicate that the region was sensitive to the B/A warm period but not to the H1 and YD cold events (Gong et al., 2019), which may be more affected by the ISM. However, the signals for H1, YD, and B/A recorded by the pollen of Xingyun Lake, located in the east of the Qinghai Tibet Plateau were relatively weak, which may be more affected by the ISM and EASM (Shen and Xiao, 2018). Therefore, the southwest of the Sichuan Basin may be more affected by the EASM, especially when the ISM is relatively weak.

The gradual temperature rises during the last deglaciation may have been predominantly affected by the gradual increase in low-latitude summer solar radiation since ∼21 kyr BP (**Figure 7E**), which in turn led to the strengthening of the

ISM (Shen and Xiao, 2018). The millennial-scale cooling events (H1 and YD) may have been related to the weakening of the monsoon in response to the weakening of the Atlantic Meridional Overturning Circulation (AMOC), which would have changed the sea surface temperature (Broecker, 2003; Mohtadi et al., 2014, 2016; An et al., 2015). The monsoon began to increase significantly during the B/A, and the emergence of the B/A warm period may be related to the significant increase in radiative forcing produced by greenhouse gases dominated by $CO_2$ during this period (Clark et al., 2012; Hong et al., 2014).

### Holocene climate characteristics

The climate of the Holocene (since 11.2 cal kyr BP) was generally warm and humid, with intensified climate fluctuations. It can be seen from **Figure 6** that TOC increases first and then decreases between 11.2 and 7.5 cal kyr BP, the $\delta^{13}$Corg value showed a gradually higher trend, and the Al/Si ratio fluctuated rapidly, especially reaching the minimum value of about 9.0 cal kyr BP. These changes reflect the climate generally cooled and showed significant fluctuations during the early Holocene (11.2–7.5 cal kyr BP); this is in contrast to the slow and early temperature increase in the Holocene that is reflected by the sporopollen records of Qinghai and Lugu Lake, Yunnan (Xiao et al., 2015; Shen and Xiao, 2018), and to the rapid rise in temperature in the Holocene reflected by the sporopollen records of Wuxu Lake, which is closer to the EASM area (Zhang et al., 2016). Several paleoenvironmental records (Chen et al., 2015; Jia et al., 2015; Zhang, 2017; Kang et al., 2020) in the EASM area indicate a generally warm and humid climate of the early Holocene, which is likely related to the relatively strong EASM during this period. The difference in early Holocene climate characteristics in Southwest China may be related to the relatively strong EASM and the fact that some areas were simultaneously affected by both the EASM and ISM. Therefore, climate change during this period shows regional and complex characteristics.

The Holocene Megathermal is from 7.5 to 3.5 cal kyr BP in the GC records. During this period, the climate was the warmest and wettest, but the climate fluctuation intensified. The environmental indicators in **Figure 6** have obvious responses to climate change in this period. Especially at ∼6.0 cal kyr BP, TOC, $\delta^{13}$Corg, Al/Si, and K/Ti ratio showed the most obvious fluctuations since the Holocene, suggesting that this was the most serious climate fluctuation event during the Holocene Megathermal, which is consistent with the results of the Baoan peat records (Hong et al., 2018; **Figure 7B**) in the adjacent area. The climate cooling in the Middle Holocene is also believed to be closely related to the origin and development of civilization in the Chengdu Plain area in the western Sichuan Basin. Under this climate background, some ancient people from the upper reaches of the Minjiang River migrated to the Chengdu Plain and gave birth to Baodun culture (Huang et al., 2019). The peat records in the east of the QTP also indicate that the 6.0 cal kyr BP climate cooling event is more significant than the 8.2 ka event, which is likely related to the sudden weakening of the EASM around 6.2 kyr BP (Yu et al., 2006). The paleoclimate records of the GC core suggest that the Holocene Megathermal mainly occurred during the mid-Holocene (**Figure 7**), which is consistent with the timing observed in other records of the surrounding ISM areas (Xiao et al., 2015; Zhang et al., 2018; **Figures 7C,E**). The Holocene Megathermal timing in our record also lagged that of most EASM areas, which appeared to have started in the early Holocene (Dykoski et al., 2005; Chen et al., 2015; **Figure 7B**). The Holocene evolution of the EASM and ISM was mainly controlled by the changes in the equatorial Intertropical Convergence Zone (ITCZ), which gradually migrated southward under the control of summer solar insolation in the Northern Hemisphere (Dong et al., 2006). Since the Holocene, the summer solar insolation in the Northern Hemisphere has continually decreased. However, the Holocene Megathermal in Southwest China lags behind the peak solar radiation, which may be related to the continuous melting of glaciers after the solar radiation peak, resulting in a rise in the sea level (Griffiths et al., 2009) and sea surface temperatures (Overpeck et al., 1996). In addition, the research (Yan, 2022) shows that the enhancement of glacier ablation caused by the temperature rise in the middle Holocene exceeded the increase of glacier accumulation caused by the increase of precipitation, which led to the significant retreat of glaciers in Asia's alpine regions during this period. Therefore, during the Holocene Megathermal, the western Sichuan Basin became wetter due to the melting of glaciers on the QTP.

The research area experienced a cooling period in the late Holocene after 3.5 cal kyr BP. TOC and $\delta^{13}$Corg in the GC core recorded a strong cooling event at ∼1.0 cal kyr BP, which was also recorded in the Baoan peatland and Qinghai Lake (**Figure 7**). However, the GC core did not significantly respond to the 4.2 cal kyr BP cooling event, which is the most detected late-Holocene cooling event globally.

## Conclusion

The sedimentary environment and hydroclimate evolution of the southern margin of the Sichuan Basin since the LGM were reconstructed from the Ganchi wetland core based on concentrations in major and trace elements, TOC, and $\delta^{13}$Corg. During LGM(26.2–18.2 cal kyr BP), the climate is cold and dry, and the study area was a wetland sedimentary environment. Except for some aquatic plants, C3 vegetation began to dominate from this stage. Since the last deglaciation (18.2–10.9 cal kyr BP), the sedimentary environment of Ganchi transitioned from wetland to peatland, and the C3 vegetation further increased, while the aquatic plants decreased. Peat started to develop in Ganchi at ∼13.7 cal kyr BP, which coincided with the

first peak of peat development in the Hengduan Mountains. During the last deglaciation, the climate in the study area was generally warm but was affected by several abrupt climate events. Similarly, the climate of the Holocene (since 11.2 cal kyr BP) was generally warm and humid, with intensified climate fluctuations.

The hydroclimate in the southwest Sichuan Basin since the LGM showed similar regional evolution characteristics to that observed in Southwest China from the LGM to the Holocene, but exhibited local and more complex climatic characteristics during the Holocene. The climate of the LGM was cold and dry, and the first warming period after the LGM occurred at 18.2 cal kyr BP, which was consistent with the timing of the first warming period in other records of Southwest China. The climate warmed during the last deglaciation, and the abrupt cooling during H1, B/A, and YD was detected in the GC core. Affected by the topography of the QTP, The climate change pattern during the last deglaciation in the southwestern margin of the Sichuan Basin is mainly affected by the EASM and less affected by the ISM. During the Holocene, the climate was generally warm and humid, but the climate fluctuation intensified. The early Holocene climate may have been affected by both the ISM and the EASM, resulting in more complex local climate characteristics. The timing of the Holocene Megathermal (7.5–3.5 cal kyr BP) in our record was consistent with its timing in other records of the ISM region. The climatic cooling event during this period was closely related to the beginning of Baodun Culture in the Chengdu Plain. The research area then entered a cold period during the late Holocene.

## Data availability statement

The original contributions presented in this study are included in the article/supplementary material, further inquiries can be directed to the corresponding author.

## Author contributions

MH and CM designed the study. MH, CM, HP, YD, and HG analyzed the data. CM and HP performed the analyses and revised the manuscript. ZW and GS did the fieldwork. MH and ZW completed the laboratory analysis. MH wrote the manuscript. All authors contributed to interpreting the results and discussions.

## Funding

This research was jointly supported by the National Natural Science Foundation of China (Nos. 41977389 and 42271173), the Frontiers Science Center for Critical Earth Material Cycling Fund (No. JBGS2102), and the National Key Research and Development Program of China (Nos. 2020YFC1521605, 2020YFC1521603, and 2020YFC1521606).

## Acknowledgments

We thank Chenglong Li and Bin Zhou from the School of Earth Sciences and Engineering, Nanjing University for their guidance in laboratory analysis. We also thank the Natural Resources Bureau of Jinkouhe District, Leshan City, Sichuan Province for supporting our field sampling.

## Conflict of interest

The authors declare that the research was conducted in the absence of any commercial or financial relationships that could be construed as a potential conflict of interest.

## Publisher's note



## References

Alley, R. B., and Clark, P. U. (1999). The deglaciation of the Northern hemisphere: A global perspective. *Annu. Rev. Earth Planet. Sci.* 27, 149–182. doi: 10.1146/annurev.earth.27.1.149

An, Z., Wu, G., Li, J., Sun, Y., Liu, Y., Zhou, W., et al. (2015). Global monsoon dynamics and climate change. *Annu. Rev. Earth Planet. Sci.* 43, 2.1–2.49. doi: 10.1146/annurev-earth-060313-054623

Babek, O., Grygar, T. M., Famera, M., Hron, K., Novakova, T., and Sedlacek, J. (2015). Geochemical background in polluted river sediments: How to separate the effects of sediment provenance and grain size with statistical rigour? *Catena* 135, 240–253. doi: 10.1016/j.catena.2015.07.003

Berger, A., and Loutr, M. F. (1991). Insolation values for the climate of the last 10 million years. *Quat. Sci. Rev.* 10, 297–317. doi: 10.1016/0277-3791(91)90033-Q

Blaauw, M., and Christen, J. A. (2011). Flexible paleoclimate age-depth models using an autoregressive gamma process. *Bayesian Anal.* 6, 457–474. doi: 10.1214/11-BA618

Blackford, J. (2000). Palaeoclimatic records from peat bogs. *Trends Ecol. Evol.* 15, 193–198. doi: 10.1016/S0169-5347(00)01826-7

Bloemsma, M. R., Zabel, M., Stuut, J. B. W., Tjallingii, R., Collins, J. A., and Weltje, G. (2012). Model-ling the joint variability of grain size and chemical composition in sediments. *Sediment. Geol.* 280, 135–148. doi: 10.1016/j.sedgeo.2012.04.009

Broecker, W. S. (2003). Does the trigger for abrupt climate change reside in the ocean or in the atmosphere? *Science* 300, 1519–1522. doi: 10.1126/science.1083797

Chambers, F. M., Booth, R. K., De Vleeschouwer, F., Lamentowicz, M., Le Roux, G., Mauquoy, D., et al. (2012). Development and refinement of proxy-climate indicators from peats. *Quat. Int.* 268, 21–33. doi: 10.1016/j.quaint.2011.04.039

Chambers, F. M., and Charman, D. J. (2004). Holocene environmental change: Contributions from the peatland archive. *Holocene* 14, 1–6. doi: 10.1191/0959683604hl684ed

Chen, F., Xu, Q., Chen, J., Birks, H. J., Liu, J., Zhang, S., et al. (2015). East Asian summer monsoon precipitation variability since the last deglaciation. *Sci. Rep.* 5:11186. doi: 10.1038/srep11186

Cheng, A., Yu, J., Zhang, L., Liu, Y., and Gao, C. (2011). Analysis of Toson Lake XRF core scanning and application of multivariate statistical methods. *J. Saltlake Res.* 19, 20–25.

Clark, P. U., Dyke, A. S., Shakun, J. D., Carlson, A. E., Clark, J., Wohlfarth, B., et al. (2009). The last glacial maximum. *Science* 325, 710–714. doi: 10.1029/2005GC001226

Clark, P. U., Shakun, J. D., Baker, P. A., Bartlein, P. J., Brewer, S., Brook, E., et al. (2012). Global climate evolution during the last deglaciation. *Proc. Natl. Acad. Sci. U.S.A.* 109, E1134–E1142. doi: 10.1073/pnas.1116619109

Cook, C. G., Leng, M. J., Jones, R. T., Langdon, P. G., and Zhang, E. (2012). Lake ecosystem dynamics and links to climate change inferred from a stable isotope and organic palaeorecord from a mountain lake in Southwestern China (ca. 22.6–10.5 cal kyr BP). *Quat. Res.* 77, 132–137. doi: 10.1016/j.yqres.2011.09.011

Cuven, S., Francus, P., and Lamoureux, S. F. (2010). Estimation of grain size variability with micro X-ray fluorescence in laminated lacustrine sediments, Cape Bounty, Canadian High Arctic. *J. Paleolimnol.* 44, 803–817. doi: 10.1007/s10933-010-9453-1

Deng, Y. K., Ma, C. M., Huang, M., Zhao, L., Shang, G. C., Tang, L. Y., et al. (2022). Vegetation and climate changes since the Last Glacial Maximum inferred from high-resolution pollen records from the Sichuan Basin, Southwest China. *Paleogeogr. Paleoclimatol. Paleoecol.* 606:111231. doi: 10.1016/j.palaeo.2022.111231

Denton, G. H., Anderson, R. F., Toggweiler, J. R., Edwards, R. L., Schaefer, J. M., and Putnam, A. E. (2010). The last glacial termination. *Science* 328, 1652–1654. doi: 10.1126/science.1184119

Devry, I. J. (1993). Pollen evidence of changing Holocene monsoon climate in Sichuan province, China. *Quat. Res.* 39, 325–337. doi: 10.1006/qres.1993.1039

Díaz, K. A., Pérez, L., Correa-Metrio, A., Franco-Gaviria, J. F., Echeverría, P., Curtis, J., et al. (2017). Holocene environmental history of tropical, mid-altitude Lake Ocotalito, México, inferred from ostracodes and non-biological indicators. *Holocene* 27, 1308–1317. doi: 10.1177/0959683616687384

Dong, J., Kong, X., and Wang, Y. (2006). The East Asian Monsoon climate changes at mt. shennongjia and its relation to shift of intertropical convergence zone during the Holocene. *Quat. Sci.* 26, 827–834.

Dykoski, C., Edwards, R., Cheng, H., Yuan, D., Cai, Y., Zhang, M., et al. (2005). A high-resolution, absolute-dated Holocene and deglacial Asian monsoon record from Dongge Cave, China. *Earth Planet. Sci. Lett.* 233, 71–86. doi: 10.1016/j.epsl.2005.01.036

Francey, R. J., and Farquhar, G. D. (1982). An explanation of 13C/12C variations in tree rings. *Nature* 297, 28–31. doi: 10.1038/297028a0

Gong, X., Chen, C., Tang, Y., Huang, K., Yue, Y., Liang, K., et al. (2019). Palaeoenvironment changes during the past 21 kyr inferred from organic geochemical records of Caohai Lake,Guizhou Province. *J. Palaeogeogr.* 21, 1025–1034.

Govil, P., and Divakar Naidu, P. (2011). Variations of Indian monsoon precipitation during the last 32kyr reflected in the surface hydrography of the Western Bay of Bengal. *Quat. Sci. Rev.* 30, 3871–3879. doi: 10.1016/j.quascirev.2011.10.004

Griffiths, M. L., Drysdale, R. N., Gagan, M. K., Zhao, J. X., Ayliffe, L. K., Hellstrom, J. C., et al. (2009). Increasing Australian–Indonesian monsoon rainfall linked to early Holocene sea-level rise. *Nat. Geosci.* 2, 636–639. doi: 10.1038/ngeo605

Haug, G. H., Hughen, K. A., Sigman, D. M., Peterson, L. C., and Röhl, U. (2001). Southward migration of the intertropical convergence zone through the holocene. *Science* 293, 1304–1308. doi: 10.1126/science.1059725

Hennekam, R., and de Lange, G. (2012). X-ray fluorescence core scanning of wet marine sediments: Methods to improve quality and reproducibility of high-resolution paleoenvironmental records. *Limnol. Oceanogr. Methods* 10, 991–1003. doi: 10.4319/lom.2012.10.991

Hakanson, L., and Jansson, M. (2002). *Principles of lake sedimentology*. Caldwell, NJ: The Blackburn Press.

Hong, B., Hong, Y., Uchida, M., Shibata, Y., Cai, C., Peng, H., et al. (2014). Abrupt variations of Indian and East Asian summer monsoons during the last deglacial stadial and interstadial. *Quat. Sci. Rev.* 97, 58–70. doi: 10.1016/j.quascirev.2014.05.006

Hong, B., Hong, Y. T., Lin, Q. H., Shibata, Y., Uchida, M., Zhu, Y. X., et al. (2010). Anti-phase oscillation of Asian monsoons during the Younger Dryas period: Evidence from peat cellulose $\delta^{13}C$ of Hani, Northeast China. *Palaeogeogr. Palaeoclimatol. Palaeoecol.* 297, 214–222. doi: 10.1016/j.palaeo.2010.08.004

Hong, B., Uchida, M., Hong, Y., Peng, H., Kondo, M., and Ding, H. (2018). The respective characteristics of millennial-scale changes of the India summer monsoon in the Holocene and the Last Glacial. *Palaeogeogr. Palaeoclimatol. Palaeoecol.* 496, 155–165. doi: 10.1016/j.palaeo.2018.01.033

Huang, M., Zhu, C., Ma, C., He, K., and Xu, J. (2019). Paleoenvironmental context of the evolution of the Baodun Culture at Chengdu Plain, Sichuan Province, China. *Holocene* 29, 1731–1742. doi: 10.1177/0959683619862031

Huo, W. (2022). Sanxingdui: A dialogue between eastern and western ancient bronze civilizations. *J.Tsinghua Uni.* 37, 1–8.

Jia, G., Bai, Y., Yang, X., Xie, L., Wei, G., Ouyang, T., et al. (2015). Biogeochemical evidence of Holocene East Asian summer and winter monsoon variability from a tropical maar lake in southern China. *Quat. Sci. Rev.* 111, 51–61. doi: 10.1016/j.quascirev.2015.01.002

Jin, Z., An, Z., Yu, J., Li, F., and Zhang, F. (2015). Lake Qinghai sediment geochemistry linked to hydroclimate variability since the last glacial. *Quat. Sci. Rev.* 122, 63–73. doi: 10.1016/j.quascirev.2015.05.015

Johnsen, S. J., Clausen, H. B., Dansgaard, W., Fuhrer, K., Gundestrup, N., Hammer, C. U., et al. (1992). Irregular glacial interstadials recorded in a new Greenland ice core. *Nature* 359, 311–313. doi: 10.1038/359311a0

Kang, S., Du, J., Wang, N., Dong, J., Wang, D., Wang, X., et al. (2020). Early Holocene weakening and mid-to late Holocene strengthening of the East Asian winter monsoon. *Geology* 48, 1043–1047. doi: 10.1130/G47621.1

Kido, Y., Koshikyrwa, T., and Tada, R. (2006). Rapid and quantitative major element analysis method for wet fine-grained sediments using an XRF microscanner. *Mar. Geol.* 229, 209–225. doi: 10.1016/j.margeo.2006.03.002

Lamb, A. L., Wilson, G. P., and Leng, M. J. (2006). A review of coastal palaeoclimate and relative sea-level reconstructions using $\delta^{13}C$ and C/N ratios in organic material. *Earth Sci. Rev.* 75, 29–57. doi: 10.1016/j.earscirev.2005.10.003

Lawrence, F. W., and Upchurch, S. B. (1982). Identification of recharge areas using geochemical factor analysis. *Ground Water* 20, 680–687. doi: 10.1111/j.1745-6584.1982.tb01387.x

Lei, G., Zhu, Y., Jiang, X., Li, Z., Jin, J., Fang, K., et al. (2014). Climate Variations over the past 1400 Years Inferred from an α-cellulose $\delta^{13}C$ Record from Xianshan Peat in Southeast China. *Sci. Geogeaph. Sin.* 34, 1018–1024.

Li, K., Tan, B., Ni, J., and Liao, M. N. (2018). Hydroclimate changes since Last Glacial Maximum: Geochemical evidence from Yilong Lake, Southwestern China. *Acta Ecol. Sin.* 38, 8973–8982. doi: 10.5846/stxb201806011228

Liang, L., Sun, Y., Yao, Z., Liu, Y., and Wu, F. (2012). Evaluation of high-resolution elemental analyses of Chinese loess deposits measured by X-ray fluorescence core scanner. *Catena* 92, 75–82. doi: 10.1016/j.catena.2011.11.010

Liu, B., Sheng, E., Lan, J., and Yu, K. (2022). Peat development in the Napahai wetland and its response to variations in the intensity of the Indian summer monsoon, southwestern China, since the last deglaciation. *Palaeogeogr. Palaeoclimatol. Palaeoecol.* 598:111026. doi: 10.1016/j.palaeo.2022.111026

Liu, G. (2016). Formation and evolution mechanism of ecological security pattern in Southwest China. *Acta Ecol. Sin.* 36, 7088–7091. doi: 10.5846/stxb201611212364

Liu, L., Chen, H., Yu, Z., Zhu, D., He, Y., Liu, J., et al. (2020). Peatland development and carbon dynamics since the Last Glacial Maximum in the Hengduan Mountains Region. *Catena* 190:104525. doi: 10.1016/j.catena.2020.104525

Loring, D. H., and Asmund, G. (1996). Geochemical factors controlling accumulation of major and trace elements in Greenland coastal and fjord sediments. *Environ. Geol.* 28, 2–11. doi: 10.1007/s002540050072

Luo, C. (2003). Geomorphological study on Jinkou Grand Canyon and Dawa mountain area. *J. Leshan Nom. Coll.* 18, 84–88.

Ma, X., Chen, D., Yang, Y., Zhang, Y., and Zhang, J. (2014). Statistical analysis of XRF scanned elements and their environmental significance in Hala lake, Qinghai, China. *J. Saltlake Res.* 22, 1–10.

Meng, Q., Niu, R., Zheng, X., Zhou, L., Sun, C., and Wang, L. (2018). Geochemical characteristics of the peat profile in the Yangbajing basin, Tibetan, China and its paleoenvironmental implications. *J. East China Norm. Univ.* 151–159.

Meyers, P. A. (1994). Preservation of elemental and isotopic source identification of sedimentary organic matter. *Chem. Geol.* 114, 289–302. doi: 10.1016/0009-2541(94)90059-0

Meyers, P. A. (1997). Organic geochemical proxies of paleoceanographic, paleolimnologic, and paleoclimatic processes. *Org. Geochem.* 27, 213–250. doi: 10.1016/S0146-6380(97)00049-1

Meyers, P. A., and Ishiwatari, R. (1993). Lacustrine organic geochemistryman overview of indicators of organic matter sources and diagenesis in lake sediments. *Org. Geochem.* 20, 867–900. doi: 10.1016/0146-6380(93)90100-P

Meyers, P. A., and Lallier-Vergès, E. (1999). Lacustrine sedimentary organic matter records of Late Quaternary paleoclimates. *J. Paleolimnol.* 21, 345–372. doi: 10.1023/A:1008073732192

Mohtadi, M., Prange, M., Oppo, D. W., De Pol-Holz, R., Merkel, U., Zhang, X., et al. (2014). North Atlantic forcing of tropical Indian Ocean climate. *Nature* 509, 76–80. doi: 10.1038/nature13196

Mohtadi, M., Prange, M., and Steinke, S. (2016). Palaeoclimatic insights into forcing and response of monsoon rainfall. *Nature* 533, 191–199. doi: 10.1038/nature17450

Morrill, C., Overpeck, J. T., Cole, J. E., Liu, K. B., Shen, C., and Tang, L. (2006). Holocene variations in the Asian monsoon inferred from the geochemistry of lake sediments in central Tibet. *Quat. Res.* 65, 232–243. doi: 10.1016/j.yqres.2005.02.014

O'Leary, M. H. (1981). Carbon isotope fractionation in plants. *Phytochemistry* 20, 553–567. doi: 10.1016/S0016-7037(60)80006-3

O'Leary, M. H. (1988). Carbon Isotopes in Photosynthesis: Fractionation techniques may reveal new aspects of carbon dynamics in plants. *Bioscience* 38, 328–336. doi: 10.2307/1310735

Overpeck, J., Anderson, D., Trumbore, S., and Prell, W. (1996). The southwest Indian Monsoon over the last 18000 years. *Clim. Dynam.* 12, 213–225. doi: 10.1007/BF00211619

Peng, H., Bao, K., Yuan, L., Uchida, M., Cai, C., Zhu, Y., et al. (2021). Abrupt climate variability since the last deglaciation based on a high-resolution peat dust deposition record from southwest China. *Quat. Sci. Rev.* 252:106749. doi: 10.1016/j.quascirev.2020.106749

Peros, M., Collins, S., G'Meiner, A. A., Reinhardt, E., and Pupo, F. M. (2017). Multistage 8.2 kyr event revealed through high-resolution XRF core scanning of Cuban sinkhole sediments. *Geophys. Res. Lett.* 44, 7374–7381. doi: 10.1002/2017GL074369

Qu, H., and Huang, B. (2019). Paleoclimate change reflected by element ratios of terrigenous sediments from deep-sea Oxygen isotope MIS6 to MIS5 at MD12-3432 stationinnorthern South China Sea. *Earth Sci. Front.* 26, 236–242.

Reimer, P. J., Bard, E., Bayliss, A., Beck, J. W., Blackwell, P. G., Ramsey, C. B., et al. (2013). IntCal13 and Marine13 radiocarbon age calibration curves 0-50,000 Years cal BP. *Radiocarbon* 55, 1869–1887. doi: 10.2458/azu_js_rc.55.16947

Shakun, J. D., and Carlson, A. E. (2010). A global perspective on Last Glacial Maximum to Holocene climate change. *Quat. Sci. Rev.* 29, 1801–1816. doi: 10.1016/j.quascirev.2010.03.016

Shen, J. (2013). Spatiotemporal variations of Chinese lakes and their driving mechanisms since the Last Glacial Maximum: A review and synthesis of lacustrine sediment archives. *Chin. Sci. Bull* 58, 17–31. doi: 10.1007/s11434-012-5510-7

Shen, J., and Xiao, X. (2018). Evolution of the South Asian monsoon during the last 20 kyr recorded in lacustrine sediments from Southwestern China. *Quat. Sci.* 38, 799–820.

Stuiver, M., and Grootes, P. M. (2000). GISP2 oxygen isotope ratios. *Quat. Res.* 53, 277–284. doi: 10.1006/qres.2000.2127

Talbot, M. R., and Laerdal, T. (2000). The Late Pleistocene-Holocene palaeolimnology of Lake Victoria, East Africa, based upon elemental and isotopic analyses of sedimentary organic matter. *J. Paleolimnol.* 23, 141–164. doi: 10.1023/A:1008029400463

Wang, D., and Chen, X. (2014). The Development and Control of Geohazards in Jinkouhe Town. *Leshan. Acta Geol. Sichuan* 34, 416–420.

Wang, H., Hong, Y., Lin, Q., Hong, B., Zhu, Y., Wang, Y., et al. (2010). Response of humification degree to monsoon climate during the Holocene from the Hongyuan peat bog, eastern Tibetan Plateau. *Palaeogeogr. Palaeoclimatol. Palaeoecol.* 286, 171–177. doi: 10.1016/j.palaeo.2009.12.015

Wang, Q., Yang, X., Anderson, N. J., Zhang, E., and Li, Y. (2014). Diatom response to climate forcing of a deep, alpine lake (Lugu Hu, Yunnan, SW China) during the Last Glacial Maximum and its implications for understanding regional monsoon variability. *Quat. Sci. Rev.* 86, 1–12. doi: 10.1016/j.quascirev.2013.12.024

Wang, Y. J., Cheng, H., Edwards, R. L., An, Z. S., Wu, J. Y., Shen, C. C., et al. (2001). A High-resolution absolute-dated late pleistocene monsoon record from Hulu Cave, China. *Science* 294, 2345–2348. doi: 10.1126/science.1064618

Weltje, G. J., and Tjallingii, R. (2008). Calibration of XRF core scanners for quantitative geochemical logging of sediment cores: Theory and application. *Earth Planet. Sci. Lett.* 274, 423–438. doi: 10.1016/j.epsl.2008.07.054

Wersin, P., Hohener, P., Giovanoli, R., and Stumm, W. (1991). Early diagenetic influences on iron transformations in a freshwater lake sediment. *Chem. Geol.* 90, 233–252. doi: 10.1016/0009-2541(91)90102-W

Wu, D., Zhou, A., Chen, X., Yu, J., Zhang, J., and Sun, H. (2015). Hydrological and ecosystem response to abrupt changes in the Indian monsoon during the last glacial, as recorded by sediments from Xingyun Lake, Yunnan, China. *Palaeogeogr. Palaeoclimatol. Palaeoecol.* 421, 15–23. doi: 10.1016/j.palaeo.2015.01.005

Wu, X., Shen, J., and Wang, Y. (2011). Holocene paleoenvironmental evolution of the Huguangyan maar lake. *Mar. Geol. Quat. Geol.* 31, 155–162. doi: 10.3724/SP.J.1140.2011.04155

Xiao, X., Haberle, S. G., Shen, J., Yang, X., Han, Y., Zhang, E., et al. (2014a). Latest Pleistocene and Holocene vegetation and climate history inferred from an alpine lacustrine record, northwestern Yunnan Province, southwestern China. *Quat. Sci. Rev.* 86, 35–48. doi: 10.1016/j.quascirev.2013.12.023

Xiao, X., Haberle, S. G., Yang, X., Shen, J., Han, Y., and Wang, S. (2014b). New evidence on deglacial climatic variability from an alpine lacustrine record in northwestern Yunnan Province, Southwestern China. *Palaeogeogr. Palaeoclimatol. Palaeoecol.* 406, 9–21. doi: 10.1016/j.palaeo.2014.04.008

Xiao, X., Shen, J., Haberle, S. G., Han, Y., Xue, B., Zhang, E., et al. (2015). Vegetation, fire, and climate history during the last 18 500 cal a BP in southwestern Yunnan Province, China. *J. Quat. Sci.* 30, 859–869. doi: 10.1002/jqs.2824

Xing, W., Bao, K. S., Gallego-Sala, A. V., Charman, D. J., Zhang, Z., Gao, C., et al. (2015) . Climate controls on carbon accumulation in peatlands of Northeast China. Quat. Sci. Rev. 115, 78Ű88. doi: 10.1016/j.quascirev.2015.03.005

Xu, H., Hong, Y., Lin, Q., Zhu, Y., Hong, B., and Jiang, H. (2006). Temperature responses to quasi-100-yr solar variability during the past 6000 years based on $\delta^{18}O$ of peat cellulose in Hongyuan, eastern Qinghai–Tibet plateau, China. *Palaeogeogr. Palaeoclimatol. Palaeoecol.* 230, 155–164. doi: 10.1016/j.palaeo.2005.07.012

Xue, J., Zhong, W., and Cao, J. (2014). Changes in C3 and C4 plant abundances reflect climate changes from 41,000 to 10,000yr ago in northern Leizhou Peninsula, South China. *Palaeogeogr. Palaeoclimatol. Palaeoecol.* 396, 173–182. doi: 10.1016/j.palaeo.2014.01.003

Yan, Q. (2022). Climate change and the associated glacier response in High-Mountain Asia during the mid-Holocene: Amodeling study. *Earth Sci. Front.* 29, 372–381.

Yang, S., and Li, C. (1999). Multiple statistic study of element geochemical characteristics-element geochemical study on the Changjiang and Huanghe sendiments. *J. Mineral Petrol.* 19, 63–67.

Yu, X., Zhou, W., Franzen, L. G., Xian, F., Cheng, P., and Jull, A. J. T. (2006). High resolution peat records for Holocene monsoon history in the eastern Tibetan Plateau. *Sci. China Ser. D Earth Sci.* 49, 615–621. doi: 10.1007/s11430-006-0615-y

Zhang, E., Sun, W., Chang, J., Ning, D., and Shulmeister, J. (2018). Variations of the Indian summer monsoon over the last 30 000 years inferred from a pyrogenic carbon record from south-west China. *J. Quat. Sci.* 33, 131–138. doi: 10.1002/jqs.3008

Zhang, W., Zhang, J., and Fan, G. (2015b). Evaluation and projection of dry- and wet-season precipitation in southwestern China using CMIP5 models. *Chin. J. Atmos. Sci.* 39, 559–570.

Zhang, E., Sun, W., Zhao, C., Wang, Y., Xue, B., and Shen, J. (2015a). Linkyrges between climate, fire and vegetation in southwest China during the last 18.5kyr based on a sedimentary record of black carbon and its isotopic composition. *Palaeogeogr. Palaeoclimatol. Palaeoecol.* 435, 86–94. doi: 10.1016/j.palaeo.2015.06.004

Zhang, X., Zhang, C., Wu, D., and Zhou, A. (2015c). Element geochemistry of lake deposits measured by X-ray fluorescencecore scanner in northwest China. *Mar. Geol. Quat. Geol.* 35, 163–174.

Zhang, E., Wang, Y., Sun, W., and Shen, J. (2016). Holocene Asian monsoon evolution revealed by a pollen record from an alpine lake on the Southeastern margin of the Qinghai–Tibetan Plateau, China. *Clim. Past.* 12, 415–427. doi: 10.5194/cp-12-415-2016

Zhang, E., Zhao, C., Xue, B., Liu, Z., Yu, Z., Chen, R., et al. (2017). Millennial-scale hydroclimate variations in southwest China linked to tropical Indian Ocean since the Last Glacial Maximum. *Geology* 45, 435–438. doi: 10.1130/G38309.1

Zhang, J. (1988). Basic climatic features in Southwest China and their causes. *J. Southwest Norm. Univ.* 153–164. doi: 10.13718/j.cnki.xsxb.1988.01.025

Zhang, W. C. (2017). *Peatland sediments and Asian summer monsoon evolution in Dajiuhu Basin since the Last Glacial Maximum*. Ph.D. dissertation. Xi,an: Institute of Earth Environment, Chinese Academy of Sciences.

Zhao, L., Ma, C., Tang, L., Liu, K. B., Mao, L., Zhang, Y., et al. (2016). Investigation of peat sediments from Daiyun Mountain in southeast China: Late Holocene vegetation, climate and human impact. *Veg. Hist. Archaeobot.* 25, 359–373. doi: 10.1007/s00334-016-0554-2

Zhao, Y., Yu, Z., and Zhao, W. (2011). Holocene vegetation and climate histories in the eastern Tibetan Plateau: Controls by insolation-driven temperature or monsoon-derived precipitation changes? *Quat. Sci. Rev.* 30, 1173–1184. doi: 10.1016/j.quascirev.2011.02.006

Zheng, D., and Li, B. (1990). Evolution and differentation of the physico-geographical environment of Qinghai-Xizang Plateau. *Geogr. Res.* 9, 1–10.

Zhou, B., Wali, G., Peterse, F., and Bird, I. M. (2016). Organic carbon isotope and molecular fossil records of vegetation evolution in central Loess Plateau since 450 kyr. *Sci. China Earth. Sci.* 59, 1–10. doi: 10.1007/s11430-016-5276-x

Zhou, W., Lu, X., Wu, Z., Deng, L., Jull, A. J. T., Donahue, D., et al. (2002). Peat record reflecting Holocene climatic change in the Zoigê Plateau and AMS radiocarbon dating. *Chin. Sci. Bull.* 47, 66–70.

Zhu, L., Lu, X., Wang, J., Peng, P., Kyrsper, T., Daut, G., et al. (2015). Climate change on the Tibetan Plateau in response to shifting atmospheric circulation since the LGM. *Sci. Rep.* 5:13318. doi: 10.1038/srep13318

Zhu, Z., Mo, J., Zhang, W., Chen, J., and Zeng, Y. (2010). Oxygen isotopic composition of cellulose in sediments from lake Caohai, and its paleoenvironmental implications. *Earth Environ.* 38, 8–13.